American Journal of Applied Chemistry
2017; 5(1): 7-18
http://www.sciencepublishinggroup.com/j/ajac
doi: 10.11648/j.ajac.20170501.12
ISSN: 2330-8753 (Print); ISSN: 2330-8745 (Online)

A Comprehensive Analytical Evaluation of the Trivedi Effect® - Energy of Consciousness Healing Treatment on the Physical, Structural, and Thermal Properties of Zinc Chloride

Mahendra Kumar Trivedi[1], Alice Branton[1], Dahryn Trivedi[1], Gopal Nayak[1], Aileen Carol Lee[1], Aksana Hancharuk[1], Carola Marina Sand[1], Debra Jane Schnitzer[1], Rudina Thanasi[1], Eileen Mary Meagher[1], Faith Ann Pyka[1], Gary Richard Gerber[1], Johanna Catharina Stromsnas[1], Judith Marian Shapiro[1], Laura Nelson Streicher[1], Lorraine Marie Hachfeld[1], Matthew Charles Hornung[1], Patricia M. Rowe[1], Sally Jean Henderson[1], Sheila Maureen Benson[1], Shirley Theresa Holmlund[1], Stephen P. Salters[1], Parthasarathi Panda[2], Snehasis Jana[2, *]

[1]Trivedi Global, Inc., Henderson, Nevada, USA

[2]Trivedi Science Research Laboratory Pvt. Ltd., Bhopal, Madhya Pradesh, India

Email address:

publication@trivedieffect.com (S. Jana)

[*]Corresponding author

To cite this article:

Mahendra Kumar Trivedi, Alice Branton, Dahryn Trivedi, Gopal Nayak, Aileen Carol Lee, Aksana Hancharuk, Carola Marina Sand, Debra Jane Schnitzer, Rudina Thanasi, Eileen Mary Meagher, Faith Ann Pyka, Gary Richard Gerber, Johanna Catharina Stromsnas, Judith Marian Shapiro, Laura Nelson Streicher, Lorraine Marie Hachfeld, Matthew Charles Hornung, Patricia M. Rowe, Sally Jean Henderson, Sheila Maureen Benson, Shirley Theresa Holmlund, Stephen P. Salters, Parthasarathi Panda, Snehasis Jana. A Comprehensive Analytical Evaluation of the Trivedi Effect® - Energy of Consciousness Healing Treatment on the Physical, Structural, and Thermal Properties of Zinc Chloride. *American Journal of Applied Chemistry.* Vol. 5, No. 1, 2017, pp. 7-18. doi: 10.11648/j.ajac.20170501.12

Received: January 31, 2017; **Accepted**: February 13, 2017; **Published**: February 25, 2017

Abstract: Zinc chloride has an importance in pharmaceutical and nutraceutical industries for the prevention and treatment of several diseases. The objective of the current study was to investigate the impact of The Trivedi Effect® - Energy of Consciousness Healing Treatment (Biofield Energy Treatment) on physical, structural, and thermal properties of zinc chloride using PXRD, PSD, FT-IR, UV-vis, TGA, and DSC analysis. Zinc chloride was divided into two parts – one part was control, while other part was treated with The Trivedi Effect® remotely by eighteen renowned Biofield Energy Healers and defined as The Trivedi Effect® Treated sample. A significant change of the crystallite size and relative intensities of the PXRD peaks was observed in The Trivedi Effect® treated sample with respect to the control sample. The average crystallite size of the treated sample was significantly increased by 41.22% compared with the control sample. The size of the particles at d_{10}, d_{50}, and d_{90} was increased by 8.33%, 6.27%, and 1.83%, respectively in the treated sample compared with the control sample. The surface area of the treated sample was decreased by 5.90% compared with the control sample. The FT-IR spectroscopic analysis revealed that Zn-Cl stretching in the control and treated sample were at 511 and 507 cm^{-1}, respectively. The UV-vis analysis exhibited that wavelength of the maximum absorbance of both the control and treated samples were at 196.4 and 196.3 nm, respectively. The TGA analysis exhibited that weight loss of the treated sample was reduced by 13.98% and 2.43% in the 1st and 2nd steps of degradation, respectively. Consequently, the DSC analysis revealed that the maximum thermal decomposition temperature of the treated sample (489.06°C) was significantly increased by 15.75% compared with the control sample (422.50°C). Moreover, a significant increase in the enthalpy of decomposition was noticed in the treated sample (ΔH_{decomp} = 131.40 J/g) by 137.10% compared with the control sample (ΔH_{decomp} = 55.42 J/g). The current study anticipated that The Trivedi Effect® Treatment might lead to produce a new polymorphic form of zinc chloride, which could have better powder flowability and thermal stability. The treated sample could be more stable during manufacturing, delivery or storage conditions than the untreated sample. Hence, the treated zinc chloride would be very useful to design better nutraceutical and/or

pharmaceutical formulations that might offer better therapeutic response against inflammatory diseases, immunological disorders, aging, stress, cancer, etc.

Keywords: Consciousness Energy Healing Treatment, Biofield Energy Healers, The Trivedi Effect®, Zinc Chloride, PXRD, Particle Size, Surface Area, TGA, DSC

1. Introduction

Zinc is a vital mineral element in human and animal nutrition with a wide array of biological activities. It plays an important roles in catalytic, structural or regulation in greater than 200 zinc metalloenzymes identified in the biological systems [1, 2]. These enzymes are involved in the nucleic acid and protein metabolism as well as for the production of energy. Zinc also maintains the structural integrity of the biological membranes resulting in their protection against oxidative injury [1]. As a metallotherapeutic agent, zinc possesses various pharmacological activities include fertility enhancing, retino-protective, and putative antiviral activities [3]. Zinc is also used in the treatment of Wilson's disease [4]. It has also immunomodulatory and antioxidant activities [1]. Zinc is also used to prevent the development of several deficiency symptoms include parakeratosis, hypogeusia, anorexia, dysosmia, geophagia, hypogonadism, growth retardation, etc. [5-7]. Recently, it has been reported that zinc had increased the leukocyte count and phagocytic index, which potentiate the immunomodulatory effect along with *Glycyrrhiza glabra* [8]. Zinc chloride ($ZnCl_2$) is hygroscopic inorganic salt and highly soluble in water [9]. It is sometimes used in pharmaceutical industry as drug and diagnostic agent due to its powerful astringent and mild antiseptic properties [10]. It is also used in mouth-wash and deodorant preparations. Zinc chloride is used in as dentin desensitizer *i.e.* reduces the sensitivity of the teeth to heat and cold. The other applications of zinc chloride include protein precipitation and insulin preparation [10, 11]. Literature reported that zinc chloride has been used in the treatment of cancer as a destructive agent [12] and in the pluripotency maintenance of mouse embryonic stem cell through the regulation of STAT3 signaling pathway [13]. It can be useful for the palliative treatment of canine and malignant skin wounds [14]. It has opposite effect on locomotor behavior of rats [15]. Therefore, zinc chloride was considered as one of the component in the novel proprietary herbomineral formulation for the source of zinc ion. This herbomineral formulation is designed as nutraceutical supplement and can be used for the prevention and treatment of various human disorders.

An élan vital or vital force which contributes the 'life' is preserved by every living organisms and known as prana by the Hindus, *qi* or *chi* by the Chinese, and *ki* by the Japanese. This is believed to co-relate with the soul, spirit and mind. This hypothetical vital force is considered as the Biofield Energy. The Biofield Energy is infinite, paradimensional and dynamic electromagnetic field surrounding the human body. It can freely flow between the human and environment that leads to the continuous movement or matter of energy [16, 17]. So, a human has the ability to harness energy from the earth, the "universal energy field" and transmit it to any living or nonliving object (s) around the globe. The objects always receive the energy and respond in a useful way. This process is known as Biofield Energy Healing Treatment [18, 19]. Biofield (Putative Energy Fields) based Energy Therapies are used worldwide to promote health and healing. The National Center of Complementary and Integrative Health (NCCIH) has been recognized and accepted Biofield Energy Healing as a complementary and alternative medicine (CAM) health care approach in addition to other therapies, medicines and practices such as natural products, deep breathing, yoga, Tai Chi, Qi Gong, chiropractic/osteopathic manipulation, meditation, massage, special diets, homeopathy, progressive relaxation, guided imagery, acupressure, acupuncture, relaxation techniques, hypnotherapy, healing touch, movement therapy, pilates, rolfing structural integration, mindfulness, Ayurvedic medicine, traditional Chinese herbs and medicines, naturopathy, essential oils, aromatherapy, Reiki, cranial sacral therapy and applied prayer (as is common in all religions, like Christianity, Hinduism, Buddhism and Judaism) [20]. Biofield Energy Treatment (The Trivedi Effect®) has been reported in numerous peer-reviewed science journals with significant outcomes in many scientific fields such as cancer research [21]; altered antimicrobial sensitivity of pathogenic microbes in microbiology [22-24], biotechnology [25, 26], genetics [27, 28]; changing the structure of the atom in relation to various metals, ceramics, polymers and chemicals in materials science [29, 30], altered physical and chemical properties of pharmaceuticals [31, 32], nutraceuticals [33, 34], organic compounds [35-37], and improved overall growth and yield of plants in agricultural science [38, 39]. The physicochemical properties such as particle size, crystalline structure, crystallite size, surface area, etc. and thermal properties of a drug have a vital role in bioavailability as well as stability of the drug during processing, formulation, storage, and packaging [40, 41]. The particle size, specific surface area, crystalline nature, chemical and thermal behavior of an atom/ion might be altered by the Biofield Energy Healing Treatment (The Trivedi Effect®) through possible mediation of neutrinos [42]. By considering all these aspects, powder X-ray diffraction (PXRD), particle size distribution analysis (PSD), Fourier transform infrared (FT-IR) spectrometry, ultraviolet-visible (UV-vis) spectroscopy, thermogravimetric analysis (TGA), and differential scanning calorimetry (DSC) analytical

techniques were conducted in this study for the characterization of physical, structural, and thermal properties of the Biofield Energy Treated and untreated zinc chloride.

2. Materials and Methods

2.1. Chemicals and Reagents

Zinc chloride was procured from TCI, Japan. All other chemicals used in the experiment were of analytical grade available in India.

2.2. The Trivedi Effect® Energy of Consciousness Treatment Strategies

Zinc chloride was one of the components of the new proprietary herbomineral formulation, developed by our research team and it was used *per se* as the test compound for the current study. The test compound was divided into two parts, one part of the test compound was treated with The Trivedi Effect® - Energy of Consciousness Healing Treatment (Biofield Energy Treatment) by the renowned Biofield Energy Healers and defined as Biofield Energy Treated sample, while the second part of the test compound did not receive any sort of treatment and defined as untreated or control zinc chloride sample. This Biofield Energy Treatment was provided by the group of eighteen renowned Biofield Energy Healers who participated in this study and performed the Biofield Energy Treatment remotely. Eleven Biofield Energy Healers were remotely located in the U. S. A., four remotely located in Canada, two remotely located in Finland, and one of which was remotely located in Albania, while the test compound was located in the research laboratory of GVK Biosciences Pvt. Ltd., Hyderabad, India. This Biofield Energy Treatment was provided for 5 minutes through Healer's Unique Energy Transmission process remotely to the test compound under the laboratory conditions. None of the Biofield Energy Healers in this study visited the laboratory in person, nor had any contact with the compounds. Similarly, the control compound was subjected to "sham" healers for 5 minutes, under the same laboratory conditions. The sham healer did not have any knowledge about the Biofield Energy Treatment. After that, the Biofield Energy Treated and untreated samples were kept in similar sealed conditions and characterized thoroughly by PXRD, PSD, FT-IR, UV-visible spectroscopy, TGA, and DSC analysis.

2.3. Characterization

2.3.1. Powder X-ray Diffraction (PXRD) Analysis

The PXRD analysis was accomplished on PANalytical X'pert Pro powder X-ray diffractometer system. The X-ray of wavelength 1.54056 Å was used. The data was collected in the form of a chart of the Bragg angle (2θ) *vs.* intensity, and a detailed table containing information on peak intensity counts, d value (Å), relative intensity (%), full width half maximum (FWHM) (θ°). From the PXRD results, the crystallite size (G) was calculated using X'pert data collector and X'pert high score plus processing software. The crystallite size (G) was calculated from the Scherrer equation [43, 44]. The method was based on the width of the diffraction patterns obtained in the X-ray reflected the crystalline region. The crystallite size (G) was calculated by using the following equation 1:

$$G = k\lambda / (b\text{Cos}\theta) \quad (1)$$

Where, k is the equipment constant (0.5), λ is the X-ray wavelength (0.154 nm); b in radians is the full-width at half of the peaks and θ the corresponding Bragg angle.

Percent change in crystallite size (G) was calculated using following equation 2:

$$\%\ \text{change in crystallite size} = \frac{[G_{\text{Treated}} - G_{\text{Control}}]}{G_{\text{Control}}} \times 100 \quad (2)$$

Where, $G_{Control}$ and $G_{Treated}$ are the crystallite size of the control and Biofield Energy Treated samples, respectively.

A total of ~500 mg of the control and Biofield Energy Treated samples individually were used for the analysis and prepared by back loading technique using the sample preparation kit. The sample was spread on the holder ring in sufficient quantity to fill the ring cavity. It was then pressed down using powder press block and scrap the powder that was in surplus using a glass slide to get densely packed specimen. Consequently, the bottom plate was placed onto the holder ring and clamp in position. The sample holder was then removed from the sample preparation table by turning it upside down. A smooth surface of sample was obtained to ensure optimum results.

2.3.2. Particle Size Distribution (PSD) Analysis

The average particle size and particle size distribution were analyzed using Malvern Mastersizer 2000, UK with a detection range between 0.01 µm to 3000 µm. The sample unit was filled with the dispersant medium and operated the stirrer at 2500 rpm. Alignment of the optics was done and the background measurement was taken. After the background measurement, the sample was added into the sample unit with constant monitoring the obscuration and stopped the addition of sample when the obscuration reached in between 15% and 20%. When the obscuration was stable, the measurement was taken twice and the average was taken of two measurements. The average histogram of the two measurements was recorded. Along with histogram, the data was presented in table format which include particle size (µm). Also, the values at below 10% level (d_{10}), 50% level (d_{50}), and 90% level (d_{90}) were calculated from the histogram and the calculations such as surface area (m^2/g) were done by using software Mastersizer 2000.

Percent change in particle size (d) for at below 10% level (d_{10}), 50% level (d_{50}), and 90% level (d_{90}) was calculated using following equation 3:

$$\%\ \text{change in particle size} = \frac{[d_{\text{Treated}} - d_{\text{Control}}]}{d_{\text{Control}}} \times 100 \quad (3)$$

Where, $d_{Control}$ and $d_{Treated}$ are the particle size (μm) for at below 10% level (d_{10}), 50% level (d_{50}), and 90% level (d_{90}) of the control and Biofield Energy Treated samples, respectively.

Percent change in surface area (S) was calculated using following equation 4:

$$\% \text{ change in surface area} = \frac{[S_{Treated} - S_{Control}]}{S_{Control}} \times 100 \quad (4)$$

Where, $S_{Control}$ and $S_{Treated}$ are the surface area of the control and Biofield Energy Treated samples, respectively.

2.3.3. Fourier Transform Infrared (FT-IR) Spectroscopy

FT-IR spectroscopy of zinc chloride was performed on Spectrum two (Perkin Elmer, USA) Fourier transform infrared spectrometer with the frequency array of 400-4000 cm^{-1} by using pressed KBr disk technique.

2.3.4. Ultraviolet-Visible Spectroscopy (UV-Vis) Analysis

The UV-Vis spectral analysis was carried out using Shimadzu UV-2450 with UV Probe, Japan. The spectrum was recorded using 1 cm quartz cell that has a slit width of 1.0 nm. The wavelength range chosen for recording the spectra was 190-800 nm. The absorbance spectra (in the range of 0.2 to 0.9) and wavelength of maximum absorbance (λ_{max}) were recorded.

2.3.5. Thermal Gravimetric Analysis (TGA)

The TGA analysis was performed using Instrument TGA Q50 (TA Instruments, USA) at a heating rate of 10ºC/min from room temperature *i.e.* 30°C to 900°C under nitrogen atmosphere. A total of ~ 10 mg of sample was used for the analysis and was taken on the platinum pan. In TGA, the weight loss for each step was recorded in grams as well as in percent loss with respect to initial weight. Also, the onset, endset, and peak temperature for each step were recorded in TGA. Percent change in weight loss (W) was calculated using following equation 5:

$$\% \text{ change in weight loss} = \frac{[W_{Treated} - W_{Control}]}{W_{Control}} \times 100 \quad (5)$$

Where, $W_{Control}$ and $W_{Treated}$ are the weight loss of the control and Biofield Energy Treated samples, respectively.

2.3.6. Differential Scanning Calorimetry (DSC)

Analysis was performed using the DSC Q20 (TA Instruments, USA) differential scanning calorimeter. A total of ~7.50 mg sample was weighed and sealed in aluminum pans and equilibrated at 25°C and heated up to 600ºC at the heating rate of 10°C/min under nitrogen gas as purge atmosphere with flow rate of 50 mL/min. The value for onset, endset, peak temperature, peak height (mJ or mW), peak area, and change in heat (J/g) for each peak were recorded.

Percent change in the decomposition temperature (T) was calculated using following equation 6:

$$\% \text{ change in decomposition temperature} = \frac{[T_{Treated} - T_{Control}]}{T_{Control}} \times 100 \quad (6)$$

Where, $T_{Control}$ and $T_{Treated}$ are the decomposition temperature of the control and Biofield Energy Treated samples, respectively.

Percent change in the enthalpy of decomposition (ΔH) was calculated using following equation 7:

$$\% \text{ change in enthalpy of decomposition} = \frac{[\Delta H_{Treated} - \Delta H_{Control}]}{\Delta H_{Control}} \times 100 \quad (7)$$

Where, $\Delta H_{Control}$ and $\Delta H_{Treated}$ are the enthalpy of decomposition of the control and Biofield Energy Treated samples, respectively.

3. Results and Discussion

3.1. Powder X-ray Diffraction (PXRD) Analysis

The PXRD diffractograms of both the control and Biofield Energy Treated zinc chloride are shown in Figure 1. Very sharp and intense peaks in both the diffractograms indicating the crystalline nature of zinc chloride. PXRD data such as Bragg angle (2θ), relative intensity (%), full width half maximum (FWHM) (θ°), and crystallite size (G) for the control and Biofield Energy Treated zinc chloride are presented in Table 1. The crystallite size was calculated with the help of Scherrer equation [43, 44]. The crystallite size of the Biofield Energy Treated zinc chloride at 2θ equal to nearly 16.6°, 25.4°, 29.4°, 35.0°, 38.3°, 58.4°, and 61.8° (Table 1, entry 1-5, 7, and 8) was significantly increased from 25% to 133% compared with the control sample. Consequently, only at 2θ equal to ~49.3° (Table 1, entry 6), the crystallite size of the Biofield Energy Treated zinc chloride was significantly reduced by 16.68% with respect to the control sample. However, the average crystallite size of the Biofield Energy Treated sample was significantly increased by 41.22% (Table 1, entry 9) with respect to the control sample.

The PXRD diffractogram of the Biofield Energy Treated zinc chloride showed greater intensity at Bragg's angle (2θ) equal to 29.36° (Table 1, entry 3), whereas it was observed at 16.62° (Table 1, entry 1) in the control sample. Beside this, the relative intensities of the XRD peaks (Table 1) in the Biofield Energy Treated sample were significantly altered as compared to the control sample. It has been found in the scientific literature that XRD relative intensity of each diffraction face on the crystalline compound changes according to the crystal morphology [45]. Thus, it is presumed that the energy transferred through the Biofield Energy Healing probably altered the shape and size of molecules of the Biofield Energy Treated sample, which might be responsible for an alteration in the relative intensities and crystallite size in the Biofield Energy Treated sample as compared to the control sample.

Table 1. *PXRD data for the control and Biofield Energy Treated zinc chloride.*

Entry No.	Bragg angle (°2θ)		Relative Intensity (%)		FWHM (°2θ)		Crystallite size (G, nm)		
	Control	Treated	Control	Treated	Control	Treated	Control	Treated	% change*
1	16.62	16.59	100.00	49.07	0.0836	0.0669	53.21	66.49	24.96
2	25.47	25.44	66.18	80.64	0.1171	0.0502	38.54	89.89	133.26
3	29.38	29.36	67.23	100.00	0.1171	0.0816	38.86	55.77	43.50
4	34.97	35.06	76.10	41.24	0.0612	0.0408	75.42	113.16	50.04
5	38.31	38.30	41.08	44.02	0.1224	0.0816	38.08	57.12	50.00
6	49.26	49.23	47.13	42.07	0.1020	0.1224	47.49	39.57	-16.68
7	58.38	57.46	27.17	23.53	0.0816	0.0612	61.83	82.07	32.74
8	61.83	61.81	26.11	15.97	0.0816	0.0612	62.92	83.89	33.32
9	Average crystallite size						52.04	73.50	41.22

FWHM: Full width half maximum, *denotes the percentage change in the crystallite size of the Biofield Energy Treated sample with respect to the control sample.

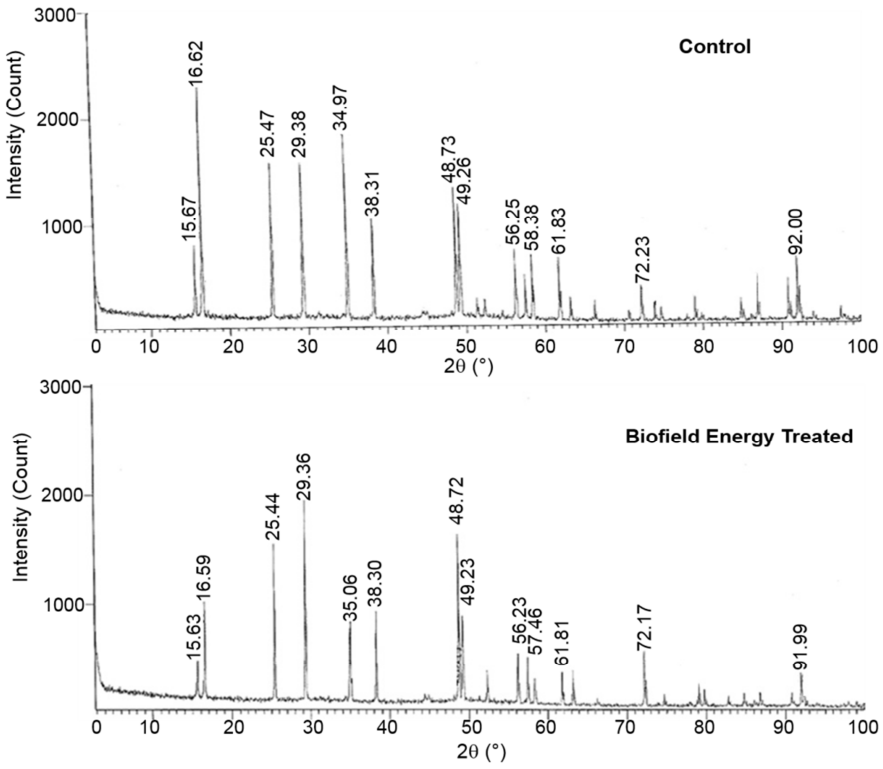

Figure 1. *PXRD diffractogram of the control and Biofield Energy Treated zinc chloride.*

Raza *et al*. reported that changes in XRD pattern provide the proof of polymorphic transitions [46, 47]. Crystal habit, size, and even polymorphic form of a drug have a significant effect on the drug solubility, dissolution, and bioavailability. It has been reported in the literature that alteration in the crystal morphology had the significant impact on *in vitro* dissolution rate, with prospective for improving bioavailability [41]. Hence, PXRD study revealed that Biofield Energy Healing Treatment might be introduced a new polymorphic form of zinc chloride, which could have improved bioavailability as compared with the control sample.

3.2. Particle Size Distribution (PSD) Analysis

The particle size data (d_{10}, d_{50}, and d_{90}) of both the control and Biofield Energy Treated zinc chloride was investigated and the results are presented in Table 2.

Table 2. *Particle size data (d_{10}, d_{50}, and d_{90}) and surface area of the control and Biofield Energy Treated zinc chloride.*

Parameter	d_{10} (µm)	d_{50} (µm)	d_{90} (µm)	Surface area (m^2/g)
Control	0.96	2.71	6.57	3.05
Biofield Energy Treated	1.04	2.88	6.69	2.87
Percent change* (%)	8.33	6.27	1.83	-5.90

*denotes the percentage change in the particle size data (d_{10}, d_{50}, and d_{90}) and surface area of the Biofield Energy Treated sample with respect to the control sample.

It was evident that Biofield Energy Treatment has the ability to enhance the particle size (d_{10}, d_{50}, and d_{90}) of zinc chloride with respect to the control sample. The size of the particles at below 10% level (d_{10}), 50% level (d_{50}), and 90% level (d_{90}) was increased by 8.33%, 6.27%, and 1.83%, respectively in the Biofield Energy Treated sample as compared to the control sample.

Particle size as well as the surface area have a major effect on dissolution of a compound in a solvent, because the surface energy influenced by surface area and chemical affinity is the driving factor for dissolution efficiency [48, 49]. The surface area for both the control and Biofield Energy Treated zinc chloride samples was analyzed and the results are presented in Table 2. The control sample showed surface area of 3.05 m^2/g and it was decreased to 2.87 m^2/g in the Biofield Energy Treated zinc chloride. The result showed 5.9% decrease in surface area of the Biofield Energy Treated sample with respect to the control sample. Kale *et al.* [50] reported that introduction of the external force leads to the transform the fine particles into larger particles. The various reasons to increase the particle size are enhanced the powder flowability, improved product shape and appearance [50]. It is presumed that the Biofield Energy Healing Treatment (*i.e.* consider as external force) might improve the powder flowability, shape and appearance of zinc chloride. XRD data also supported that the Biofield Energy Healing Treatment could alter the size, shape, and appearance of zinc chloride.

3.3. Fourier Transform Infrared (FT-IR) Spectroscopy

The FT-IR spectra of the control and Biofield Energy Treated samples of zinc chloride are presented in Figure 2.

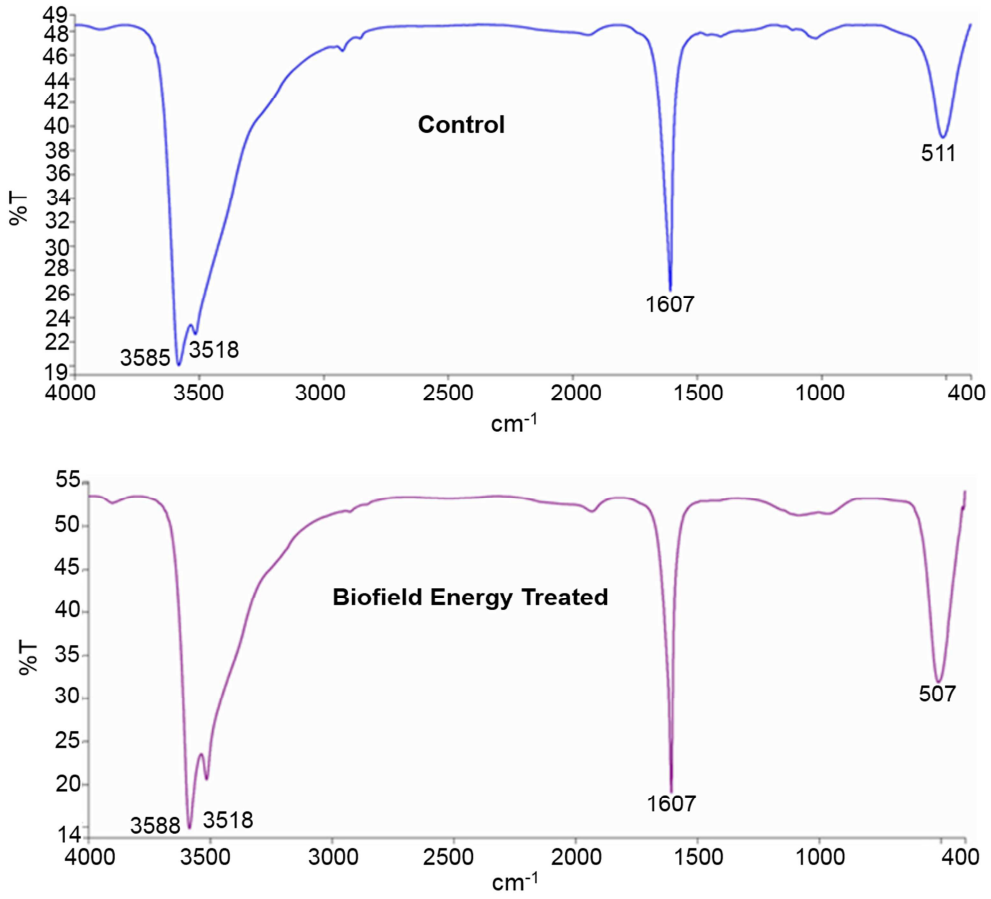

Figure 2. *FT-IR analysis of the control and Biofield Energy Treated zinc chloride.*

The peaks found in the control IR spectrum were at 3585, 3518, 1607, and 511 cm^{-1}, whereas the Biofield Energy Treated zinc chloride showed the peaks at 3588, 3518, 1607, and 507 cm^{-1}. The strong and broad absorption band centered at 3585 and 3588 cm^{-1}, while the H-O-H bending motion was noticed at 1607 cm^{-1} in the FT-IR spectra indicated the presence of the lattice water in both the control and Biofield Energy Treated zinc chloride samples. The fingerprint region of the Biofield Energy Treated and control samples was remained same. From the literature, it has been found that metal stretching absorption band for inorganic materials was found in the 750-100 cm^{-1} region [51]. In control spectrum, metal-halogen (Zn-Cl) stretching was shown at 511 cm^{-1}, whereas it was displayed in the Biofield Energy Treated sample at 507 cm^{-1}. Overall, IR peaks of the Biofield Energy Treated zinc chloride did not show any significant changes with respect to the control sample.

3.4. Ultraviolet-Visible Spectroscopy (UV-Vis) Analysis

The UV-visible spectra of the both control and Biofield Energy Treated zinc chloride are presented in Figure 3. The UV-visible spectra exhibited that the maximum absorbance (λ_{max}) of both the control and Biofield Energy Treated samples were at 196.4 and 196.3 nm, respectively with a minor shift of absorbance maxima from 1.9984 to 1.9784 in the control and Biofield Energy Treated samples, respectively. The UV absorbance occurs due to the different type of energy transitions from the singlet to the singlet excited state such as $\sigma \rightarrow \sigma^*$, $n \rightarrow \pi^*$, and $\pi \rightarrow \pi^*$. These type of electronic transitions are happened when the difference in energy between the lowest unoccupied molecular orbital (LUMO) and the highest occupied molecular orbital (HOMO) is significantly higher than the activation energy of the compound [52].

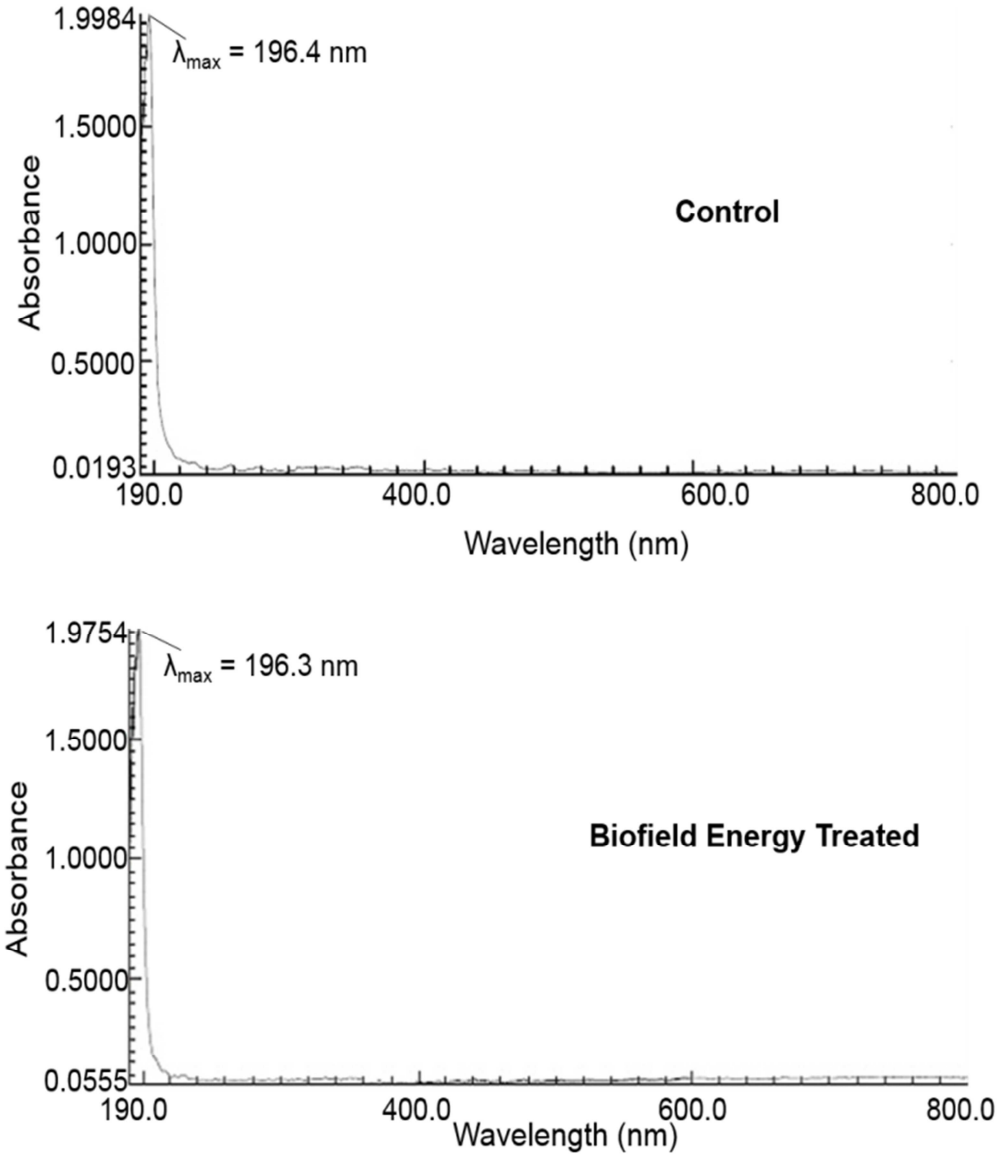

Figure 3. *UV-vis spectra of the control and Biofield Energy Treated zinc chloride.*

The UV-vis spectroscopic analysis of zinc chloride showed no change in the λ_{max} of the Biofield Energy Treated sample as compared to the control sample. Thus, the structural configuration or activation energy of the Biofield Energy Treated sample was not changed as compared to the control sample.

3.5. Thermal Gravimetric Analysis (TGA)

The TGA thermograms of both the control and Biofield Energy Treated samples are presented in Figure 4. The TGA thermogram of both the control and Biofield Energy Treated samples exhibited two steps thermal degradation and mentioned in Table 3. The pattern of the thermal degradation of the control zinc chloride was nearly matched with the reported data [53]. The weight loss of the 1st step (8.37%) and 2nd step (85.87%) degradation in the Biofield Energy Treated zinc chloride was significantly reduced by 13.98% and 2.43%, respectively as compared with the control sample (1st step = 9.73% and 2nd step = 88.01%).

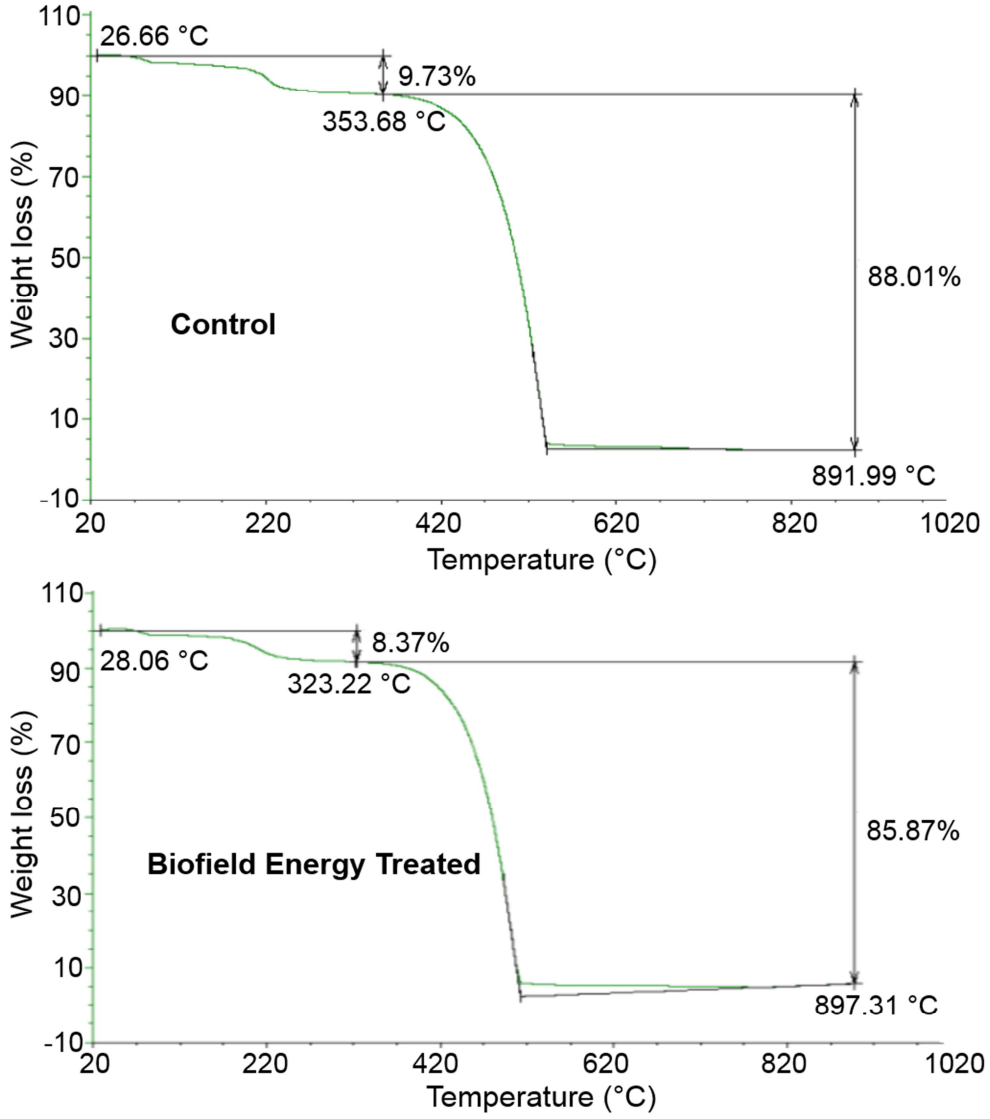

Figure 4. *TGA thermograms of the control and Biofield Energy Treated zinc chloride.*

Table 3. *Thermal degradation steps of the control and Biofield Energy Treated zinc chloride.*

Step	Temperature (°C)		% Weight loss		% Change*
	Control	Biofield Energy Treated	Control	Biofield Energy Treated	
1st step of degradation	353.68	323.22	9.73	8.37	-13.98
2nd step of degradation	891.99	897.31	88.01	85.87	-2.43
Total weight loss	-	-	97.74	94.24	-3.58

*denotes the percentage change in the weight loss of the Biofield Energy Treated sample with respect to the control sample.

The total weight loss of the Biofield Energy Treated sample (94.24%) was significantly reduced by 3.58% compared with the control sample (97.74). Overall, the TGA study revealed that the Biofield Energy Treated zinc chloride was thermally more stable as compared with the control sample.

3.6. Differential Scanning Calorimetry (DSC) Analysis

The DSC thermograms of the control and Biofield Energy Treated zinc chloride are presented in Figure 5. The decomposition temperature and enthalpy of decomposition of both the control and Biofield Energy Treated zinc chloride are presented in Table 4. A significant increase (15.75%) in the decomposition temperature (T_{decomp}) was observed in the Biofield Energy Treated zinc chloride (489.06°C) as compared to the control sample (422.50°C). The onset and endset decomposition temperatures of the Biofield Energy Treated sample were significantly increased by 16.61% and 16.05%, respectively compared with the control sample. The control zinc chloride exhibited the enthalpy decomposition of 55.42 J/g, whereas the Biofield Energy Treated sample showed 131.40 J/g. The results as shown in Table 4,

indicated a significant increase in the enthalpy of decomposition by 137.10% with respect to the control sample. It is anticipated that Biofield Energy Treatment might enhance the internal energy in zinc chloride that leads to increase in the enthalpy of decomposition as well as thermal stability of the Biofield Energy Treated sample.

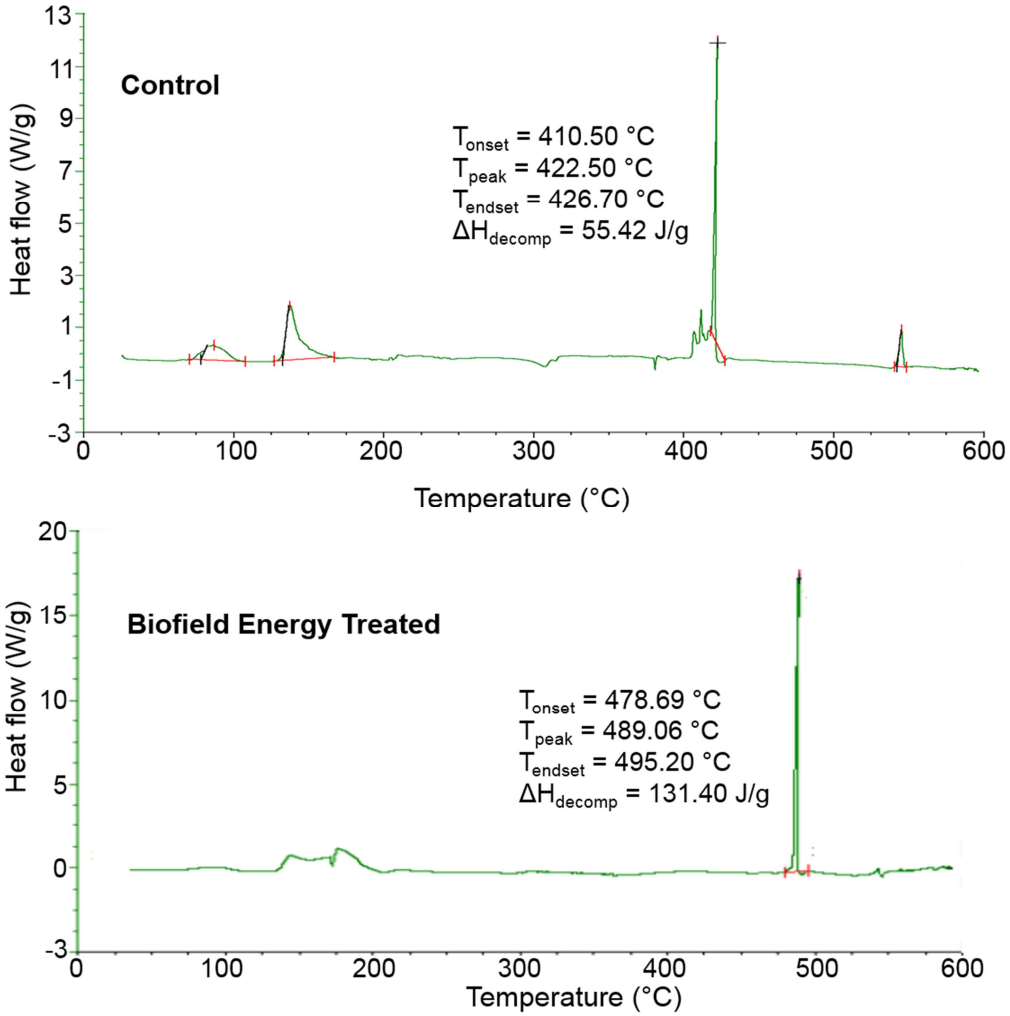

Figure 5. *DSC thermograms of the control and Biofield Energy Treated zinc chloride.*

The enhanced thermal stability of a drug is an advantage in the maintenance of the product in long term storage condition throughout the shelf-life for any pharmaceutical formulations [54].

Table 4. *The enthalpy of decomposition (J/g) and decomposition temperature (°C) values of the control and Biofield Energy Treated zinc chloride.*

Sample	Enthalpy of decomposition (ΔH_{decomp}) J/g	Onset decomposition temperature (T_{onset})°C	Peak decomposition temperature (T_{peak})°C	Endset decomposition temperature (T_{endset})°C
Control	55.42	410.50	422.50	426.70
Biofield Energy Treated	131.40	478.69	489.06	495.20
% Change[a]	137.10	16.61	15.75	16.05

T_{onset}: Onset decomposition temperature, T_{peak}: Peak decomposition temperature, T_{endset}: Endset decomposition temperature, $\Delta H_{decomposition}$: Enthalpy of decomposition, [a]denotes the percentage change of the Biofield Energy Treated sample with respect to the control sample.

4. Conclusions

The current study revealed that the Biofield Energy Healing Treatment (The Trivedi Effect®) had the notable effects on the physicochemical and thermal properties of zinc chloride. The PXRD data displayed the significant alteration of the crystallite size and relative intensities of the XRD peaks in The Trivedi Effect® sample with respect to the control sample. The average crystallite size of The Trivedi Effect® Treated sample was significantly enhanced by 41.22% with respect to the control sample. The particle size analysis indicated a significant increment in the particle size of the treated zinc chloride at d_{10}, d_{50}, and d_{90} by 8.33%, 6.27%, and 1.83%, respectively with respect to the control sample. Consequently, the surface area analysis

indicated 5.9% reduction in surface area of the treated sample with respect of the control sample. The weight loss of the treated zinc chloride in 1st and 2nd step degradation was significantly decreased by 13.98% and 2.43%, respectively compared with the control sample. The DSC analysis exhibited a significant increase in the decomposition temperature by 15.75%, along with a noticeable enhancement of the enthalpy of decomposition by 137.10% in the treated zinc chloride with compared with the control sample. The TGA and DSC analysis exhibited that the treated zinc chloride was found to be thermally more stable compared with the control sample. Briefly, The Trivedi Effect® - Energy of Consciousness Healing Treatment might introduce a new thermally stable polymorphic form of zinc chloride that can have improved powder flowability, size, and appearance. The treated sample could be more stable during manufacturing, delivery or storage conditions than the untreated sample. Hence, the Biofield Energy Treated zinc chloride would be very useful to design better nutraceutical and/or pharmaceutical formulations that might offer better therapeutic response against inflammatory diseases, immunological disorders, aging, stress, cancer, Wilson's disease, viral diseases, parakeratosis, hypogeusia, anorexia, dysosmia, geophagia, hypogonadism, growth retardation, etc.

Abbreviations

DSC: Differential scanning calorimetry, FT-IR: Fourier transform infrared spectroscopy, FWHM: Full width half maximum, G: Crystallite size, HOMO: Highest energy occupied molecular orbital, LUMO: Lowest energy unoccupied molecular orbital, TGA: Thermal gravimetric analysis, T_{onset}: Onset decomposition temperature, T_{peak}: Peak decomposition temperature, T_{endset}: Endset decomposition temperature, $\Delta H_{decomposition}$: Enthalpy of decomposition, UV-vis: Ultraviolet-visible spectroscopy, PSD: Particle size distribution; PXRD: Powder X-ray diffraction.

Acknowledgements

The authors gratefully acknowledged to GVK Biosciences Pvt. Ltd., Trivedi Science, Trivedi Global, Inc. and Trivedi Master Wellness for the assistance and support during the work.

References

[1] Ronconi L, Sadler PJ (2008) Applications of heteronuclear NMR spectroscopy in biological and medicinal inorganic chemistry. Coordn Chem Rev 252: 2239-2277.

[2] Berg JM, Shi Y (1996) The galvanization of biology: A growing appreciation for the roles of zinc. Science 271: 1081-1085.

[3] Higdon JV, Ho E (2005) In: M. Gielen, E. R. T. Tiekink (Eds.), Metallotherapeutic drugs and metal-based diagnostic agents: The use of metals in medicine, Wiley-VCH, Weinheim, p. 237.

[4] *Brewer GJ (2001) Zinc acetate for the treatment of Wilson's disease. Expert Opin Pharmacother 2: 1473-1477.*

[5] Prasad AS (1979) Clinical, biochemical, and pharmacological role of zinc. Ann Rev Pharmacol Toxicol 19: 393-426.

[6] Supuran CT (2008) Carbonic anhydrases: Novel therapeutic applications for inhibitors and activators. Nat Rev Drug Dis 7: 168-181.

[7] Elmes ME (1975) Letter: Zinc in human medicine. Lancet 2: 549.

[8] Mazumder PM, Pattnayak S, Parvani H, Sasmal D, Rathinavelusamy P (2012) Evaluation of immunomodulatory activity of *Glycyrhiza glabra* L. roots in combination with zing. Asian Pac J Trop Biomed 2: S15-S20.

[9] Brynestad J, Yakel HL (1978) Preparation and structure of anhydrous zinc chloride. Inorg Chem 17: 1376-1377.

[10] Kasture AV, Wadodkar SG (2008) A text book of pharmaceutical chemistry-1, Nirali Prakashan, 25th Ed., Pune, India.

[11] Mahadik KR, Kuchekar BS (2008) Concise inorganic pharmaceutical chemistry, Nirali Prakashan, 25th Ed., Pune, India.

[12] *McDaniel S, Goldman GD (2002) Consequences of using escharotic agents as primary treatment for nonmelanoma skin cancer. Arch Dermatol 138: 1593-1596.*

[13] Hu J, Yang Z, Wang J, Yu J, Guo J, Liu S, Qian C, Song L, Wu Y, Cheng J (2016) Zinc chloride transiently maintains mouse embryonic stem cell pluripotency by activating Stat3 signaling. PLoS One 11: e0148994.

[14] Fukuyama Y, Kawarai S, Tezuka T, Kawabata A, Maruo T (2016) The palliative efficacy of modified Mohs paste for controlling canine and feline malignant skin wounds. Vet Q 1: 1-7.

[15] Yakimovskii AF, Kryzhanovskaya SY (2015) Zinc chloride and zinc acetate injected into the neostriatum produce opposite effect on locomotor behavior of rats. Bull Exp Biol Med 160: 281-282.

[16] Stenger VJ (1999) Bioenergetic fields. Sci Rev Alternative Med 3: 16-21.

[17] Rogers, M (1989) "Nursing: A Science of Unitary Human Beings." In J. P. Riehl-Sisca (ed.) Conceptual Models for Nursing Practice. 3rd Edn. Norwark: Appleton & Lange.

[18] Rosa L, Rosa E, Sarner L, Barrett S (1998) A close look at therapeutic touch. Journal of the American Medical Association 279: 1005-1010.

[19] Warber SL, Cornelio D, Straughn, J, Kile G (2004) Biofield energy healing from the inside. J Altern Complement Med 10: 1107-1113.

[20] Koithan M (2009) Introducing complementary and alternative therapies. J Nurse Pract 5: 18-20.

[21] Trivedi MK, Patil S, Shettigar H, Mondal SC, Jana S (2015) The potential impact of biofield treatment on human brain tumor cells: A time-lapse video microscopy. J Integr Oncol 4: 141.

[22] Trivedi MK, Patil S, Shettigar H, Gangwar M, Jana S (2015) An evaluation of biofield treatment on susceptibility pattern of multidrug resistant *Stenotrophomonas maltophilia*: An emerging global opportunistic pathogen. Clin Microbiol 4: 211.

[23] Trivedi MK, Patil S, Shettigar H, Gangwar M, Jana S (2015) An effect of biofield treatment on multidrug-resistant *Burkholderia cepacia*: A multihost pathogen. J Trop Dis 3: 167.

[24] Trivedi MK, Patil S, Shettigar H, Bairwa K, Jana S (2015) Phenotypic and biotypic characterization of *Klebsiella oxytoca*: An impact of biofield treatment. J Microb Biochem Technol 7: 203-206.

[25] Trivedi MK, Branton A, Trivedi D, Nayak G, Mondal SC, Jana S (2015) Antibiogram, biochemical reactions and genotyping characterization of biofield treated *Staphylococcus aureus*. American Journal of BioScience 3: 212-220.

[26] Trivedi MK, Branton A, Trivedi D, Nayak G, Bairwa K, Jana S (2015) Physical, thermal, and spectroscopic characterization of biofield energy treated potato micropropagation medium. American Journal of Bioscience and Bioengineering 3: 106-113.

[27] Trivedi MK, Branton A, Trivedi D, Nayak G, Mondal SC, Jana S (2015) Biochemical differentiation and molecular characterization of biofield treated *Vibrio parahaemolyticus*. American Journal of Clinical and Experimental Medicine 3: 260-267.

[28] Trivedi MK, Branton A, Trivedi D, Gangwar M, Jana S (2015) Antimicrobial susceptibility, biochemical characterization and molecular typing of biofield treated *Klebsiella pneumoniae*. J Health Med Inform 6: 206.

[29] Trivedi MK, Tallapragada RM, Branton A, Trivedi D, Nayak G, Latiyal O, Jana S (2015) Analysis of physical, thermal, and structural properties of biofield energy treated molybdenum dioxide. International Journal of Materials Science and Applications 4: 354-359.

[30] Trivedi MK, Tallapragada RM, Branton A, Trivedi D, Nayak G, Latiyal O, Jana S (2015) Characterization of atomic and physical properties of biofield energy treated manganese sulfide powder. American Journal of Physics and Applications 3: 215-220.

[31] Trivedi MK, Branton A, Trivedi D, Nayak G, Saikia G, Jana S (2015) Physical and structural characterization of biofield treated imidazole derivatives. Nat Prod Chem Res 3: 187.

[32] Trivedi MK, Tallapragada RM, Branton A, Trivedi D, Nayak G, Mishra RK, Jana S (2015) Characterization of physical, spectral and thermal properties of biofield treated 1, 2, 4-Triazole. J Mol Pharm Org Process Res 3: 128.

[33] Trivedi MK, Tallapragada RM, Branton A, Trivedi D, Nayak G, Mishra RK, Jana S (2015) Biofield treatment: A potential strategy for modification of physical and thermal properties of gluten hydrolysate and ipomoea macroelements. J Nutr Food Sci 5: 414.

[34] Trivedi MK, Nayak G, Patil S, Tallapragada RM, Jana S, Mishra RK (2015) Bio-field Treatment: An effective strategy to improve the quality of beef extract and meat infusion powder. J Nutr Food Sci 5: 389.

[35] Trivedi MK, Branton A, Trivedi D, Nayak G, Latiyal O, Jana S (2015) Evaluation of biofield treatment on atomic and thermal properties of ethanol. Organic Chem Curr Res 4: 145.

[36] Trivedi MK, Branton A, Trivedi D, Nayak G, Singh R, Jana S (2015) Physical, thermal and spectroscopic studies on biofield treated *p*-dichlorobenzene. Biochem Anal Biochem 4: 204.

[37] Trivedi MK, Branton A, Trivedi D, Nayak G, Bairwa K, Jana S (2015) Physicochemical and spectroscopic characterization of biofield energy treated *p*-anisidine. Pharm Anal Chem Open Access 6: 102.

[38] Trivedi MK, Branton A, Trivedi D, Nayak G, Gangwar M, Jana S (2015) Agronomic characteristics, growth analysis, and yield response of biofield treated mustard, cowpea, horse gram, and groundnuts. International Journal of Genetics and Genomics 3: 74-80.

[39] Trivedi MK, Branton A, Trivedi D, Nayak G, Gangwar M, Jana S (2015) Analysis of genetic diversity using simple sequence repeat (SSR) markers and growth regulator response in biofield treated cotton (*Gossypium hirsutum* L.). American Journal of Agriculture and Forestry 3: 216-221.

[40] Chereson R (2009) Bioavailability, bioequivalence, and drug selection. In: Makoid CM, Vuchetich PJ, Banakar UV (Eds) Basic pharmacokinetics (1st Edn) Pharmaceutical Press, London.

[41] Blagden N, de Matas M, Gavan PT, York P (2007) Crystal engineering of active pharmaceutical ingredients to improve solubility and dissolution rates. Adv Drug Deliv Rev 59: 617-630.

[42] Trivedi MK, Mohan TRR (2016) Biofield energy signals, energy transmission and neutrinos. American Journal of Modern Physics 5: 172-176.

[43] Alexander L, Klug HP (1950) Determination of crystallite size with the X-Ray Spectrometer. J App Phys 21: 137.

[44] Langford JI, Wilson AJC (1978) Scherrer after sixty years: A survey and some new results in the determination of crystallite size. J Appl Cryst 11: 102-113.

[45] Inoue M, Hirasawa I (2013) The relationship between crystal morphology and XRD peak intensity on $CaSO_4$. $2H_2O$. J Crystal Growth 380: 169-175.

[46] Raza K, Kumar P, Ratan S, Malik R, Arora S (2014) Polymorphism: The phenomenon affecting the performance of drugs. SOJ Pharm Pharm Sci 1: 10.

[47] Thiruvengadam E, Vellaisamy G (2014) Polymorphism in pharmaceutical ingredients a review. World Journal of Pharmacy and Pharmaceutical Sciences 3: 621-633.

[48] http://www.dissolution.com/ddg/showthread.php?2366-Surface-Area-*vs*-Particle-Size

[49] Mosharrof M, Nyström C (1995) The effect of particle size and shape on the surface specific dissolution rate of microsized practically insoluble drugs. Int J Pharm 122: 35-47.

[50] Kale VV, Gadekar S, Ittadwar AM (2011) Particle size enlargement: Making and understanding of the behavior of powder (particle) system. Syst Rev Pharm 2: 79.

[51] Stuart BH (2004) Infrared spectroscopy: Fundamentals and applications in Analytical Techniques in the Sciences. John Wiley & Sons Ltd., Chichester, UK.

[52] Hesse M, Meier H, Zeeh B (1997) Spectroscopic methods in organic chemistry, Georg Thieme Verlag Stuttgart, New York.

[53] Martin FJ, Albers H, Lambeck PV, Van de Velde GMH, Popma ThJA (1991) Luminescent thin films by the chemical aerosol deposition technology (CADT). Aerosol Sci 22: S435-S438.

[54] Bajaj S, Singla D, Sakhuja N (2012) Stability testing of pharmaceutical products. J App Pharm Sci 2: 129-138.